Available online at www.sciencedirect.com
SCIENCE DIRECT®
Journal of Solid State Chemistry 177 (2004) 4785–4799
JOURNAL OF SOLID STATE CHEMISTRY
http://elsevier.com/locate/jssc

Semiconducting thin films of zinc selenide quantum dots

Biljana Pejova,[a,*] Atanas Tanuševski,[b] and Ivan Grozdanov[a]

[a] *Institute of Chemistry, Faculty of Natural Sciences and Mathematics, Saints Cyril and Methodius University, P.O. Box 162, Arhimedova 5, 1001 Skopje, Macedonia*

[b] *Institute of Physics, Faculty of Natural Sciences and Mathematics, Saints Cyril and Methodius University, P.O. Box 162, 1000 Skopje, Macedonia*

Received 28 January 2004; received in revised form 2 June 2004; accepted 4 June 2004

Abstract

A novel chemical route for deposition of zinc selenide quantum dots in thin film form is developed. The deposited films are characterized with very high purity in crystallographic sense, and behave as typical intrinsic semiconductors. Evolution of the average crystal size, lattice constant, lattice strain and the optical properties of the films upon thermal treatment is followed and discussed. The band gap energy of as-deposited ZnSe films is blue-shifted by ≈ 0.50 eV with respect to the bulk value, while upon annealing treatment it converges to 2.58 eV. Two discrete electronic states which originate from the bulk valence band are observed in the UV-VIS spectra of ZnSe 3D quantum dots deposited in thin film form via allowed electronic transitions to the 1*S* electronic state arising from the bulk conduction band—appearing at 3.10 and 3.50 eV. The splitting between these two states is approximately equal to the spin–orbit splitting in the case of bulk ZnSe. The electronic transitions in the case of non-quantized annealed films are discussed in terms of the direct allowed band-to-band transitions with the spin–orbit splitting of the valence band of 0.40 eV. The effective mass approximation model (i.e., the Brus model) with the static relative dielectric constant of bulk ZnSe fails to predict correctly the size dependence of the band gap energy, while only a slight improvement is obtained when the hyperbolic band model is applied. However, when substantially smaller value for ε_r (2.0 instead of 8.1) is used in the Brus model, an excellent agreement with the experimental data is obtained, which supports some earlier indications that the quantum dots ε_r value could be significantly smaller than the bulk material value. The ionization energy of a deep donor impurity level calculated on the basis of the temperature dependence of the film resistivity is 0.82 eV at 0 K.

Keywords: Zinc selenide; Thin films; Quantum dots; Quantum size effects; Band gap energy; Spin–orbit splitting; Activation energy; Effective mass approximation

1. Introduction

Recently, there has been a great interest in materials science for studying semiconducting quantum dots, deposited in thin film form, both from a fundamental as well as technological point of view, since many of their physicochemical properties are substantially different from analogous properties of macroscopic solids [1,2]. The influence of quantum size effects on the electronic properties of semiconducting nanocrystals is of fundamental interest to understand how these properties evolve as the crystal size increases from molecular dimensions to a bulk material. Thin films of semiconducting quantum dots have possible use in solar cells, light-emitting diodes, electrochromic windows, batteries, etc. [3–6]. In addition, new applications of nanocrystalline thin films, based on their unusual properties, could be developed.

Continuing our work in the field of nanocrystalline semiconductors physics and chemistry [7–14], in this study we have concentrated to preparation and investigation of opto-electrical properties of zinc selenide quantum dots in thin film form. Our interest for this semiconducting compound is due to the fact that it has several properties which make it an attractive opto-electronic material. Zinc selenide is a member of $A^{II}B^{VI}$ binary semiconductors group, with wide band gap energy, transparent over a wide range of the visible spectrum and has a relatively large nonlinear optical

*Corresponding author. Fax: +389-2-3226-865.
E-mail address: biljana@iunona.pmf.ukim.edu.mk (B. Pejova).

0022-4596/$ - see front matter © 2004 Elsevier Inc. All rights reserved.
doi:10.1016/j.jssc.2004.06.011

coefficient [15]. Zinc selenide thin films are of interest in fabrication of devices in the blue or ultraviolet region, devices useful in communication systems, electroluminiscent structures compatible with large-area displays and integrated circuits [16,17]. In the recent years, zinc selenide is used in preparation of high efficiency solar cells based on environmentally friendly Cd-free thin films such as $CuInS_2$, $CuInSe_2$ or $CuInGaSe_2$ [18,19]. Compared to cadmium sulfide, zinc selenide has a better lattice match with $CuInGaSe_2$ thin film absorbers.

We have prepared zinc selenide quantum dots in thin film form using a chemical deposition method. The advantages of this method, compared to other physical methods, are good surface coverage (which is especially important for the potential application in solar cell engineering) and opportunity to nanocrystal growth. With respect to the later characteristic, the chemical deposition methods in general allow control of the crystal size by controlling the reaction system parameters (experimental conditions) and/or by physical means (post-deposition thermal treatment). In comparison to other chemical methods [20–24], the method developed in the present study is based on thermodynamically predicted experimental design, which allowed us to use a reaction system consisting of a very small number of components, i.e., excluding any unnecessary component from the growth solution. This is especially important in order to obtain the studied material as an intrinsic semiconductor with high purity in crystallographic sense, in quantum dot form.

We also present the results from the thorough studies of the optical and electrical properties of the synthesized material, with a special emphasis on the evolution of the opto-electrical properties due to crystal size increase (from molecular to bulk crystal dimensions) in the course of thermal annealing at various temperatures. We have analyzed the optical properties of the size-quantized nanocrystals in terms of the previously developed model which explicitly accounts for the valence and conduction band discretization upon crystal size decrease, and also tested the applicability of the effective mass approximation (implemented within the much quoted Brus model), as well as of the hyperbolic band model, for prediction of the opto-electronic properties of quantized and non-quantized ZnSe nanocrystals.

2. Experimental details

Zinc selenide thin films were prepared onto standard microscope glasses using a chemical deposition method. The used substrates were treated in a diluted solution of tin(II) chloride and then annealed at 200°C for about 20 min. During this substrate treatment, small and stochastically distributed crystals of tin(II) oxide are created onto the glass surface, which, afterwards, initiate heterogeneous nucleation and improve film adhesion [9].

The thin films of zinc selenide were deposited chemically using sodium selenosulfate as a chalcogenizing agent. The film growth solution was prepared from analytical-grade reagents (zinc sulfate or zinc acetate, sodium hydroxide and 80% hydrazine hydrate), whereas the precursor of selenide ions was previously synthesized by adding gray selenium to a hot solution of sodium sulfite, stirring this mixture for 1 h at 90°C and filtering the excess of gray selenium. The solution of sodium selenosulfate is relatively unstable; it has to be kept in a dark container and has to be prepared prior to the thin film deposition process. On the other hand, the sulfite ions which are present in excess in the selenosulfate solution, improve the solution stability due to their reduction properties ($E°(SO_4^{2-}/SO_3^{2-}) = -0.90$ V [25]).

The treated glass substrates were placed in a beaker containing the solution growth prepared by mixing the following solutions: 1 cm^3 $ZnSO_4$($c(ZnSO_4) = 1$ mol/dm^3) or 1 cm^3 $Zn(CH_3COO)_2$($c(Zn(CH_3COO)_2) = 1$ mol/dm^3), 15 cm^3 NaOH (c(NaOH) = 2 mol/dm^3), 5 cm^3 80% $N_2H_4 \cdot H_2O$, 20 cm^3 Na_2SeSO_3 ($c(Na_2SeSO_3) = 1$ mol/dm^3) and distilled water to a total volume of 100 cm^3. The film deposition process was carried out for 1 h at about 60°C. The terminal film thickness was about 300 nm (measured by the gravimetric and interferometric techniques, as explained in the following chapter).

3. Thin film characterization

X-ray diffraction method (XRD) with monochromatic Cu$K\alpha$ radiation was used for identification of chemical composition of deposited material in thin film form and as a bulk, as well. The diffractograms were recorded on a Philips PW 1710 diffractometer. On the basis of recorded XRD patterns and using the Debye-Scherrer formula, the average crystal size of zinc selenide (as thin film and as bulk) was estimated.

In order to investigate the optical properties of ZnSe thin film materials, the optical spectra were recorded in the spectral range from 190 to 1100 nm on a Varian CARY 50 spectrophotometer. The spectra processing was performed using the MS EXCEL software package [26].

Film thickness was determined gravimetrically and interferometrically, on the basis of recorded transmission spectra of investigated samples, using the following equation:

$$d = \frac{1}{2} \frac{\lambda_1 \lambda_2}{n(\lambda_1)\lambda_2 - n(\lambda_2)\lambda_1}, \quad (1)$$

where λ_1 and λ_2 are wavelengths of first and second interferometric maximum, while $n(\lambda_1)$ and $n(\lambda_2)$ are

refractive indexes at λ_1 and λ_2 correspondingly. The values of $n(\lambda_1)$ and $n(\lambda_2)$ are taken from the graphical dependence of n vs. λ given in Ref. [27].

To achieve ohmic contact with the thin films a silver paste was used. The non-rectifying character of the silver–zinc selenide contacts was proved on the basis of the measured current–voltage characteristics. The type of major charge carriers in the prepared films was determined by a hot probe method.

The methods of two-point, four-point probe and constant electrical field were used to measure the dark electrical resistance. In the case of *two-point probe method*, the silver electrodes were applied 1 cm in length and 1 cm apart (i.e., the length and width of thin films were 1 cm) and the values of thin film resistance were reported in "ohms per square" units.

The setup, presented in Fig. 1, was used for experimental investigation of $R = f(T)$ dependence in argon atmosphere at $P = 80\,\text{kPa}$. The setup contains a special furnace (F), a thermocouple with voltmeter (TC), variable transformer (T), a DC source and a standard resistor (R_s). The investigated thin film sample, which is characterized with surface area of $1\,\text{cm}^2$, was placed in the furnace. The furnace was heated slowly by the variable transformer (T), while the film temperature was registered on the basis of temperature dependence of thermoelectromotive force of the used Fe–Constantane thermocouple. By mathematical analysis of the electrical circuit, which contains a standard resistor with resistance R_s and the investigated thin film with dark electrical resistance R_f, the following equation is obtained:

$$R_f = \frac{U_b R_s}{U_s} \tag{2}$$

in the case where $R_s \ll R_f$ (constant field method). In Eq. (2), U_b is the applied voltage and U_s is the voltage drop at the ends of the resistor (R_s).

The mechanism of zinc selenide crystal growth was investigated using coherent light-scattering experiments.

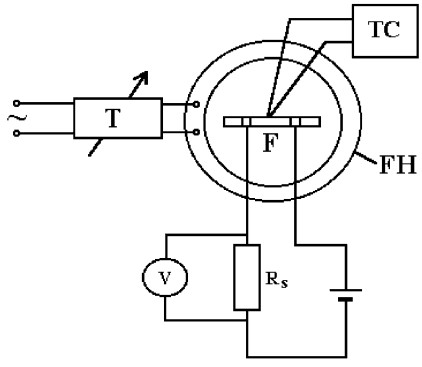

Fig. 1. The experimental setup for $R-T$ measurements.

4. Results and discussion

4.1. The chemical aspects of deposition process of ZnSe quantum dots in thin film form

In order to deposit zinc selenide quantum dots in thin film form, we have used the discovery that certain liquid phase homogeneous precipitation reactions can be controlled to give colloid particles with narrow size distributions and average diameters in the range from 1.5 to 10 nm (10^2–10^4 atoms) [28]. The liquid phase homogeneous precipitation of zinc selenide thin film materials requires the presence of a chalcogenizing agent and complexed metal ions with equilibrium stability constant value providing a concentration of metal cations in reaction system small enough to produce the controlled precipitation of films onto substrate surfaces. In this study, thin films of zinc selenide quantum dots were deposited using sodium selenosulfate as a chalcogenizing agent. The hydrolysis of selenosulfate ions is reversible:

$$SeSO_3^{2-} + H_2O = H_2Se + SO_4^{2-} \tag{3}$$

The products of this hydrolysis are a weak acid H_2Se (with acidity constant $K_a^o = 1.3 \times 10^{-15}\,\text{mol}^2\,\text{dm}^{-6}$ at 25°C [25]) and SO_4^{2-} ions. According to our experience, in acidic medium selenide ions oxidize to red selenium [29] and to prevent deposition of amorphous selenium, we have deposited ZnSe thin films in alkaline medium. In the case of alkaline aqueous solution the equilibrium of previously mentioned reaction (3) is slightly displaced to the right. But, on the other hand, the solubility product of zinc selenide is low ($K_{sp}^o \sim 10^{-31}$ [23]), so the zinc selenide precipitation can take place even at low selenide ion concentration in the reaction system. To prevent the precipitation of zinc hydroxide, zinc sulfate and zinc sulfite on the one side and to alkalize growth solution on the other side, sodium hydroxide in excess was introduced and complexed $[Zn(OH)_4]^{2-}$ ions (with instability constant $K^o = 3.6 \times 10^{-16}$ [25]) were formed in the reaction system according to the following equation:

$$Zn(OH)_{2(s)} + 2OH^- = [Zn(OH)_4]^{2-} \tag{4}$$

At the same time, the function of $[Zn(OH)_4]^{2-}$ is to control the Zn^{2+} ion concentration in solution growth and to provide controlled precipitation of zinc selenide in thin film form onto substrate surfaces. The final pH value of the deposition solution was 14.

The formation of zinc selenide takes place in accordance with the overall stoichiometric equation

$$[Zn(OH)_4]^{2-} + SeSO_3^{2-} = ZnSe + SO_4^{2-} + 2OH^- + H_2O \tag{5}$$

The experimental design of optimal conditions (initial concentrations of reactants and pH of growth solution)

was done on the basis of thermodynamic equilibriums which exist in the reaction system, also taking into account the relevant kinetics parameters and aspects. Using the experimental value for equilibrium constant of hydrolysis of selenosufate ions [30] and analyzing the following thermodynamic equilibriums:

$$[Zn(OH)_4]^{2-} = Zn^{2+} + 4OH^- \quad (6)$$

$$ZnSe_{(s)} = Zn^{2+} + Se^{2-} \quad (7)$$

(along with the corresponding kinetics aspects) the optimal experimental conditions for deposition of zinc selenide thin films (which firmly adhere to a glass substrate) were predicted. The detailed experimental design will be published elsewhere.

According to the results obtained on the basis of coherent light-scattering experiments, the zinc selenide crystals, during the most part of the deposition process, grow by cluster mechanism:

$$(ZnSe)_l + (ZnSe)_k = (ZnSe)_{l+k} \quad (8)$$

$l, k > n$ where n is the number of formula units which form a stable nucleus, which is in line with nanocrystalline film structure. The colloidal particles, formed in the reaction system, migrate to the substrate and afterwards adsorb and aggregate onto substrate surface which is in correlation with nanostructure of obtained thin films. From chemical point of view, the colloidal particles can be zinc selenide or zinc hydroxide which during deposition process converts to zinc selenide as a result of its lower solubility product.

The exact role of hydrazine in the chemical deposition of ZnSe thin films remains uncertain (although it seems possible that it could also contribute to the stability of the selenosulfate solution due to its reductive properties). It has been mentioned in a number of previous studies that it probably acts as a catalyzing agent, influencing the reaction activation energy [22,23]. However, as hydrazine has pronounced reductive properties in alkaline medium [31]:

$$N_2H_4 + 4OH^- = N_2 + 4H_2O + 4e^- \quad (9)$$

it is also possible that it initiates the generation of "free" selenide anions into the reaction system (formed by decomposition of selenosulfate ions). In such a case, its role would not be of a catalytic nature (since it would undergo a chemical change in the course of the reaction). It is anyway worth mentioning that without introduction of hydrazine hydrate in the reaction system, the precipitation of ZnSe does not occur regardless of the reaction system temperature and other initial conditions—the system remains homogeneous and purely transparent, even the precipitation of zinc hydroxide does not occur.

Our previously outlined explanation for the possible substantially important role of hydrazine for the process of ZnSe quantum dots deposition, based on its enhanced reduction properties in alkaline medium may be further supported by the following argument. The structure of selenosulfate anion is very similar to the structure of sulfate anion—except that one of the oxygen atoms in SO_4^{2-} has been replaced by selenium. The formal oxidation number of selenium in these species may be regarded as -2. However, the actual charge of selenium atom within the $SeSO_3^{2-}$ species would be expected to be significantly smaller than -2 (in absolute value) due to the larger electronegativity of the oxygen atoms. Thus, presence of a reduction agent within the deposition solution, while on one side preventing the oxidation of selenide species (obtained through decomposition of $SeSO_3^{2-}$ according to Eq. (3)) to elemental selenium, would be also expected to favor the hydrolysis of selenosulfate species.

4.2. X-ray diffraction studies

4.2.1. Identification of zinc selenide thin films by X-ray diffraction method and determination of the average crystal size by the Debye-Scherrer approach

The chemically deposited thin films of zinc selenide were identified by the X-ray diffraction method. The technique of X-ray line broadening was used for estimation of average crystal size of the obtained material in thin film form and as bulk precipitate as well. We have estimated average crystal diameter in spherical approximation from the full-width at half-maximum of more intensive diffraction peaks according to the *Debye-Scherrer* model:

$$D = \frac{4}{3}\frac{0.9\lambda}{\beta\cos\theta}, \quad (10)$$

where D is the average diameter of the crystals (in spherical approximation), λ is the wavelength of used X-ray radiation, β is the full-width at half-maximum intensity of the peak and θ is the angle which corresponds to diffraction maximum [32].

The recorded XRD patterns of as-deposited and annealed thin films and corresponding bulk precipitates, obtained using zinc sulfate as a source of Zn^{2+} ions, are presented in Fig. 2. As can be seen from the figure, the deposited material (in thin film form) is the pure cubic modification of zinc selenide with sphalerite type of structure and (bulk) unit cell parameter of 5.667 Å [33]. Upon annealing in air atmosphere, no changes in chemical composition of deposited thin films were registered.

In the case of thin film materials obtained from the bath which contains zinc acetate as a source of Zn^{2+} ions, as can be seen from Fig. 3, the as-deposited thin films and annealed ones up to 250°C (and corresponding bulk precipitates) for 1 h, are composed from cubic modification of zinc selenide, whereas upon prolonged

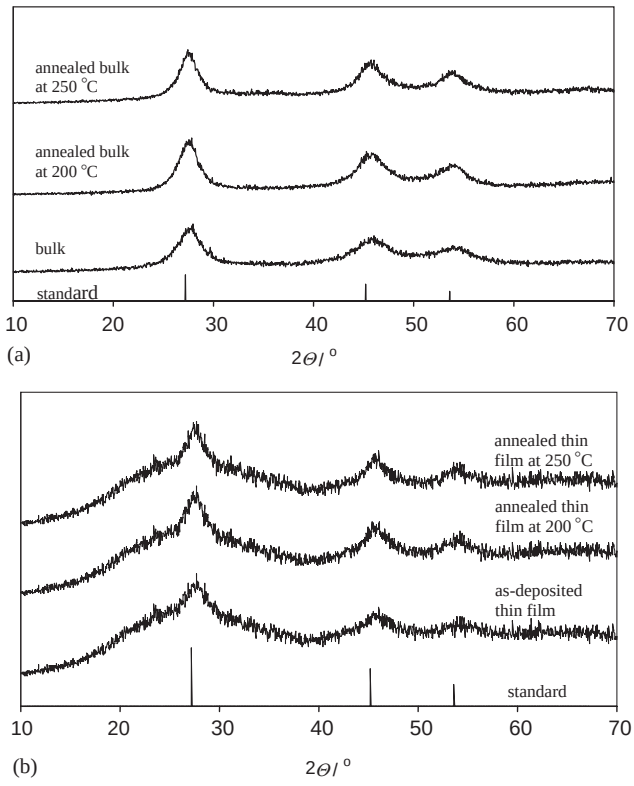

Fig. 2. XRD patterns of ZnSe samples obtained from sulfate bath: (a) bulk, (b) in thin film form.

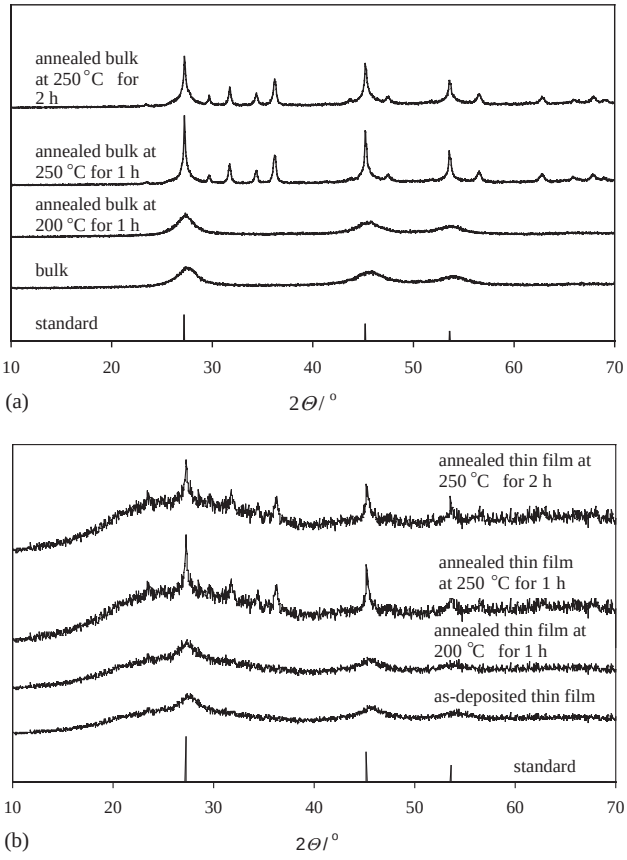

Fig. 3. XRD patterns of ZnSe samples obtained from acetate bath: (a) bulk, (b) in thin film form.

thermal treatment at 250°C, impurities of ZnO were registered.

The broad diffraction peak in the diffractograms of obtained thin films in range from 20° to 40° is due to the amorphous structure of used glass substrates.

According to the Debye-Scherrer approximation, the unannealed zinc selenide thin films, obtained from bath containing $ZnSO_4$, are nanocrystalline with average crystal radius of 1.4 nm. During annealing process, as a result of coalescence and crystal growth, the nanocrystals grow and estimated average crystal radius is 1.8 and 2.0 nm upon thermal treatments at 200°C and 250°C, correspondingly.

The estimated average crystal radius of as-deposited zinc selenide thin films, obtained from bath containing zinc acetate, is 1.8 nm. Upon annealing for about 1 h at 200°C the average crystal size increases to 2.2 nm. Figs. 2 and 3 clearly show that as particle size decreases, the line width broadens. Using the technique of X-line broadening, only the average crystal size was determined, the size distribution is unknown from this technique.

On the basis of recorded XRD patterns of obtained bulk materials, using Debye-Scherrer approximation, we have estimated their average crystal radius. The identical values with average crystal radius of corresponding zinc selenide in thin film form is in line with the previously derived conclusion that the crystal growth is carried out according to the cluster mechanism [34].

4.2.2. Determination of the lattice parameters, lattice strain and dislocation density of zinc selenide thin films by X-ray diffraction method

As the deposited ZnSe in thin film form belongs to the cubic crystallographic system, it is quite straightforward to calculate the lattice constant a on the basis of X-ray diffraction data, as well as the evolution of this parameter in the course of thermal annealing. In the case of semiconducting nanocrystalline quantum dots deposited in thin film form, the determination of lattice parameters and especially of the lattice strain arising from the large fraction of "surface atoms" and unsaturated "dangling bonds" is of substantial importance in both the fundamental sense, as well as for various applicative aspects [35].

Combining the two basic equations relating the crystal structure parameters with the observed XRD pattern in the case of cubic crystals [32]:

$$\frac{1}{d_{hkl}^2} = \frac{h^2 + k^2 + l^2}{a^2} \tag{11}$$

and:

$$n\lambda = 2d_{hkl}\sin\theta_{hkl}, \tag{12}$$

where d_{hkl} is the distance between crystallographic planes with Miller indices h, k and l, θ_{hkl} is the corresponding diffraction angle, a is the lattice constant, while λ is the wavelength of the used Cu$K\alpha$ radiation for XRD studies, and n is the reflection, i.e., diffraction order, the following expression may be easily derived for $n = 1$:

$$a = \frac{\lambda}{2}\frac{\sqrt{h^2+k^2+l^2}}{\sin\theta_{hkl}}. \tag{13}$$

On the basis of data for the two most intensive peaks in the X-ray diffractograms of as-deposited and thermally annealed ZnSe thin films, the corresponding values of the lattice constant a were calculated (along with the corresponding averages). The results are given in Table 1. As can be seen, the lattice constant a in the case of as-deposited ZnSe quantum dots in thin film form is significantly smaller than the bulk literature value, and it converges to the bulk value upon thermal annealing. Thus, the average $\Delta a = a_{\text{bulk}} - a_{\text{nanocrystal}}$ value is 0.0785 Å in the case of as-deposited ZnSe quantum dot thin films obtained from sulfate reaction solution, while it reduces to 0.0616 Å upon thermal annealing at 250°C. As shown later in this paper, this trend is accompanied with lattice strain relaxation upon thermal annealing. This convergence seems to be quite faster in the case of thin films obtained from the acetate reaction solution. Namely, if we adopt a simple definition of the isotropic average lattice strain as [36]

$$\langle\varepsilon\rangle = \frac{|\Delta a|}{a_{\text{bulk}}}, \tag{14}$$

where $\Delta a = a_{\text{bulk}} - a_{\text{nanocrystal}}$ is the difference between the bulk and nanocrystal lattice constant, then according to the previously outlined data in Table 1, the lattice strain is relaxed upon thermal annealing. A somewhat more involved treatment of the lattice strain, based on the Bragg's law may be derived as follows.

In the case of a polycrystalline aggregate in which the crystals are bent, stretched or compressed, etc., due to such lattice strains the reflections from various sets of lattice planes will be shifted with respect to the "unstrained" values. If we consider a reflection from a set of planes with the interplanar spacing d_{hkl} (in the case of an unstrained crystal), the Bragg's law for the unstrained (bulk) crystal, for the first-order reflections ($n = 1$) may be written as

$$2d_{hkl}\sin\theta_{hkl} = \lambda. \tag{15}$$

If the strain in the nanocrystal is denoted by ε, then the interplanar spacing between the previously considered set of planes will be $d_{hkl}(1+\varepsilon)$, and the corresponding Bragg angle $\theta_{hkl} + \Delta\theta_{hkl}$, leading to the following form of the Bragg's law [37]:

$$2d_{hkl}(1+\varepsilon)\sin(\theta_{hkl} + \Delta\theta_{hkl}) = \lambda. \tag{16}$$

After a few elementary trigonometric transformations, it can be easily shown that the previous expression gives

$$\Delta\theta_{hkl} = -\varepsilon\tan(\theta_{hkl}) \tag{17}$$

which allows the average lattice strain to be calculated straightforwardly from the experimental data. The ε values calculated according to this method are also presented in Table 1. As can be seen, the agreement between the values calculated by the two methods is excellent, as may be in fact a priori expected.

The dislocation density δ (defined as the overall dislocation lines length per unit crystal volume, or, equivalently, as the number of dislocations that intersect a unit area of a random section) was calculated using the

Table 1
Basic structural parameters of as-deposited and thermally annealed ZnSe thin films obtained from various Zn^{2+} ion precursors derived on the basis of XRD data

ZnSe film	2 θ (°)	*hkl*	a (Å)	$\langle a\rangle$ (Å)	$\langle R\rangle$ (nm)	δ (nm^{-2})	$\langle\varepsilon\rangle$	ε
Sulfate solution								
As-deposited	27.61	111	5.5889	5.5885	1.4	0.13	0.0139	0.0137
	45.88	220	5.5880					0.0140
Annealed at 200°C	27.51	111	5.6092	5.6033	1.8	0.08	0.0112	0.0101
	45.80	220	5.5973					0.0124
Annealed at 250°C	27.52	111	5.6071	5.6054	2.0	0.06	0.0109	0.0105
	45.74	220	5.6037					0.0113
Acetate solution								
As-deposited	27.54	111	5.6027	5.6048	1.8	0.08	0.0110	0.0113
	45.71	220	5.6068					0.0107
Annealed at 200°C	27.33	111	5.6457	5.6345	2.2	0.05	0.0057	0.0037
	45.57	220	5.6232					0.0079

expression [38]

$$\delta = \frac{n}{D^2}, \tag{18}$$

where n is a constant, with a value which is usually close to 1 [39]. The results are given in Table 1, together with all the other relevant data from structural studies. As can be seen, along with the lattice strain, the dislocation density in the case of ZnSe quantum dots deposited in thin film form also decreases upon thermally induced average crystal size increase.

4.3. Optical properties of zinc selenide thin films

4.3.1. Optical properties of as-deposited (quantum dot) thin films

According to the band theory of solid state, the band structure of semiconducting materials is a function of a three-dimensional wave vector ($\vec{k}$) within the Brillouin zone which depends on the crystal structure and corresponds to the unit cell of the reciprocal lattice. The optoelectrical properties of semiconducting materials are determined from their band structure. In order to experimentally probe the band structure of chemically deposited zinc selenide thin films and to compare the obtained conclusions with theoretically predicted ones, we have recorded the optical spectra of ZnSe thin films in the spectral range from 190 to 1100 nm. In Fig. 4, the transmission spectra of several zinc selenide thin films with different thicknesses are presented. As can be seen from this figure, the obtained thin films are characterized with high transmission, greater than 75% for wavelength values greater than ~600 nm depending on film thickness. The high transmission is in line with the fact that zinc selenide is a semiconducting material with large band gap energy. The interaction of zinc selenide thin films with electromagnetic radiation follows the equation:

$$\frac{I}{I_0} = e^{-\alpha d}, \tag{19}$$

where α is the absorption coefficient of the investigated material, d is the thickness of the thin film, while I_0 and I are the intensities of incident and transmitted light, correspondingly. The absorption coefficient (for each wavelength) was calculated by processing the recorded electronic spectra of deposited thin films according to previously mentioned equation. In Fig. 5 the dependence of absorption coefficient of as-deposited zinc selenide thin film (with thickness of 75 nm) vs. incident photon energy is presented. On the basis of presented photon energy dependence of absorption coefficient of investigated thin film sample ($\alpha = f(h\nu)$) several conclusions about band structure of zinc selenide in thin film form can be drawn. The explored spectral range (above the absorption edge at about 3 eV) is the region of intrinsic (fundamental) absorption. In this spectral range the electronic transitions from valence to conduction band produce free charge carriers (free electrons in the conduction band and free holes in the valence band). As can be seen, the absorption coefficient of zinc selenide thin film in the intrinsic region is of the order of $10^4\,cm^{-1}$ and this implies that the interband electronic transitions are based on a two-body collision (photon and electron) i.e., they are of *a direct type*. So, within the language of band theory, it can be concluded that the fundamental absorption edge of zinc selenide thin film corresponds to direct transitions from the highest valence band to the lowest conduction band at the Γ point (i.e., $\Gamma_{15}^{v} \rightarrow \Gamma_{1}^{c}$, in single group notation) [27].

The absorption spectra of ZnSe thin films show a long tail near the absorption edge (in the literature known as Urbach–Martienssen tail) which follows the following exponential function [40]:

$$\alpha = \exp[\beta(h\nu - E_g)]. \tag{20}$$

This long tail could be due to the defect states, crystal size distribution, excitons and/or indirect electron transitions. Eq. (20) implies that logarithm of α plotted as a function of E can be approximated by a straight line just below the fundamental absorption edge that converges to a point (E_0, α_0) called the "converging point". The existence of Urbach–Martienssen tails in the

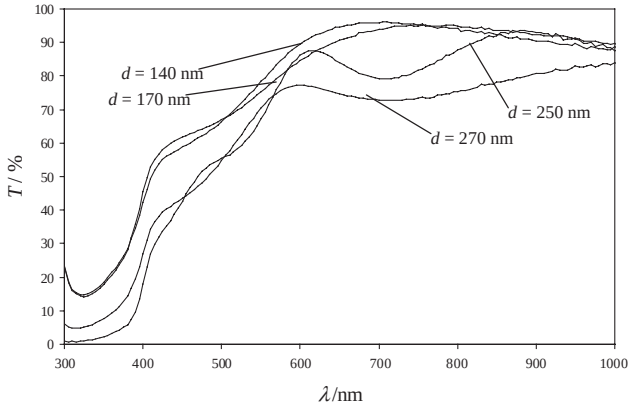

Fig. 4. Transmission spectra of several as-deposited zinc selenide thin films with different thickness (100–270 nm).

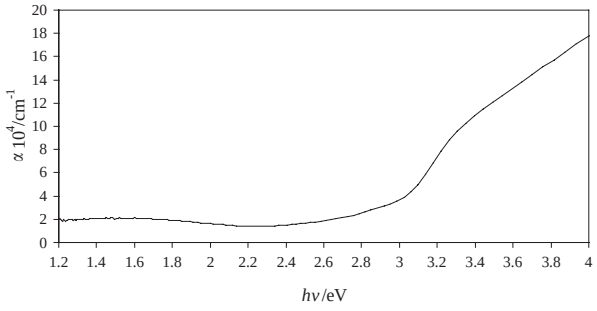

Fig. 5. Dependence of absorption coefficient of as-deposited ZnSe thin film on incident photon energy.

optical spectra of obtained zinc selenide thin films will be the subject of our next study.

To determine the direct optical band gap energy (E_g) of as-deposited thin film of zinc selenide, we fit the absorption data to the following equation:

$$(\alpha h\nu)^2 = A(h\nu - E_g), \tag{21}$$

where A is a constant which arises from the Fermi's golden rule for fundamental "band-to-band" electronic transitions within the framework of parabolic approximation for the dispersion relation [41]. Linear least-squares fits of the $(\alpha h\nu)^2$ vs. $h\nu$ dependencies were carefully carried out in the relevant energy ranges, with successive inclusion or elimination of a number of neighboring points in the correlation ranges, and parallel monitoring of the R^2 value. In this way, the sets of relevant points belonging to the linear $(\alpha h\nu)^2$ vs. $h\nu$ dependency corresponding to (or, more precisely, originating from) a given band-to-band transition were determined. Subsequent extrapolations to $\alpha h\nu = 0$ were used to obtain the corresponding transition energies, on the basis of previously derived correlation equations. All of these plots, together with the relevant statistical data are available from the authors upon request.

The $(\alpha h\nu)^2$ vs. $h\nu$ dependence of as-deposited ZnSe thin film is presented in Fig. 6. With extrapolation of linear dependence of $(\alpha h\nu)^2$ vs. $h\nu$ we have obtained a value of 3.10 eV for the band gap energy of as-deposited ZnSe thin film at room temperature. The room temperature band gap energy of bulk (microcrystalline) ZnSe is 2.58 eV [15]. The blue shift of room temperature band gap energy of 0.52 eV in the case of our chemically deposited zinc selenide thin films, compared with the corresponding value of bulk material, is due to the confinement effects, i.e., the ZnSe crystals behave as quantum dots (three-dimensionally confined structures). The zinc selenide quantum dots existence is in agreement with the average crystal size estimation on the basis of X-ray line broadening, as well as with the estimated value of the Bohr excitonic radius for bulk ZnSe given further in this paper. A preliminary quantitative treatment of the three-dimensional quantum confinement effects in the studied ZnSe quantum dots in thin film form is outlined in Section 4.4. In this section, we will focus on the description of the electromagnetic radiation absorption from ZnSe quantum dots deposited in thin film form using the modified language of the bulk band structure theory, basing on the previous works of Chestnoy et al. [28]. Besides the transition appearing at 3.10 eV, as can be seen from Fig. 6, an additional electronic transition is also observed at about 3.50 eV. The splitting between these two transitions is thus nearly 0.40 eV. The nature of these two transitions in the case of ZnSe quantum dots in thin film form, is explained below, after reviewing few basic facts regarding the bulk ZnSe band structure details, and accounting explicitly for the discrete (instead of continual) character of the energy levels in a 3D confined structure.

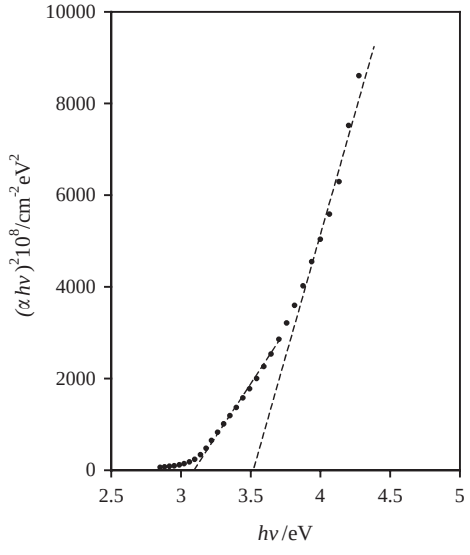

Fig. 6. Dependence of $(\alpha h\nu)^2$ on $h\nu$ in the case of as-deposited ZnSe thin film.

In order to provide a framework for assignment of the electronic transitions in the three-dimensional quantum dots of ZnSe, it is much easier to begin with a brief description of the band structure of the corresponding bulk material. The most important features of bulk ZnSe band structure (near $k = 0$) are given in Fig. 7. The conduction band is composed predominantly of metal atom s orbitals, whereas the valence band is mostly constituted of the selenide anion p ones [28]. The conduction band is thus non-degenerate and almost isotropic, while the valence band is threefold orbitally degenerate. Accounting for the spin–orbit interaction, at $k = 0$ the valence band is split into an upper (in an energetic sense) Γ_8 component, and a lower Γ_7 component. Thus, the overall degeneracy of bands, accounting for the spin degeneracy as well, is: the conduction band Γ_6 is two-fold degenerate, the valence band Γ_8 component is four-fold degenerate, while the corresponding Γ_7 component is two-fold degenerate. This language will be very useful in interpreting the electronic absorption spectra of the non-quantized ZnSe thin films (Section 4.3.2). However, in order to have a theoretical basis for assignment of the electronic transitions in the case of quantized films, the effects of size-quantization (i.e., three-dimensional quantum confinement in the present case) on the degenerate valence band have to be known. According to the model proposed by Chestnoy et al. [28], based on previous works by Baldereschi and Lipari [35], upon three-dimensional confinement of the electronic and hole motion, the following discrete energy level structure of small ZnSe clusters arises—Fig. 8. As can be seen from

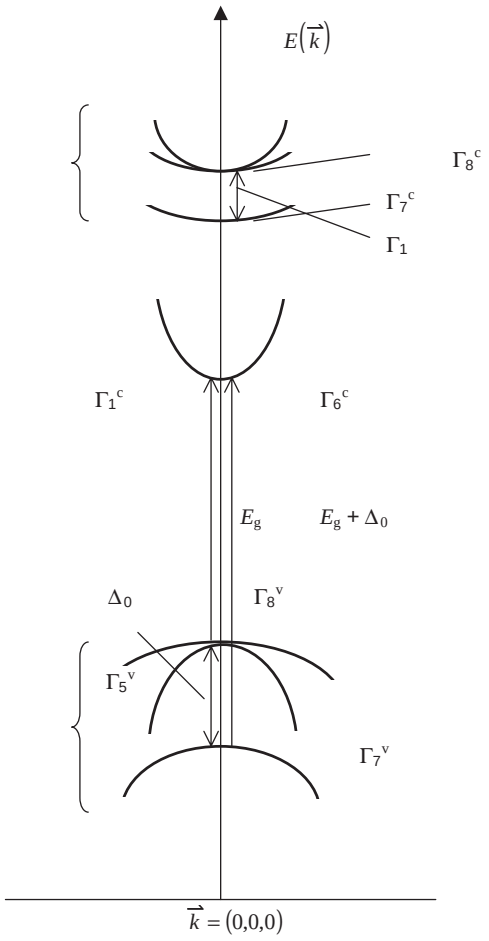

Fig. 7. Bulk zinc selenide band structure (near $k = 0$).

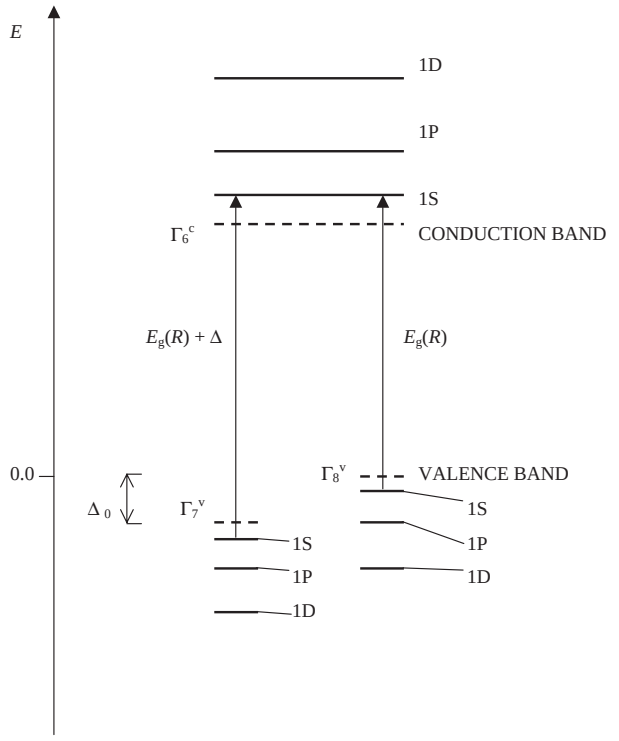

Fig. 8. Discrete energy level structure of small ZnSe clusters.

Fig. 8, this analysis predicts existence of two low lying hole states, split by a value Δ, which is expected to be similar to the Δ_{SO} (the spin–orbit splitting, usually denoted by Δ_0 as well) in the case of bulk material. These two states are indeed observed in our UV-VIS spectra of ZnSe 3D quantum dots in thin film form via allowed electronic transitions to the $1S$ electronic state arising from the bulk conduction band—these are the previously mentioned transitions at 3.10 and 3.50 eV given in Fig. 6. Such transitions are denoted by arrows in Fig. 8. The "next" allowed $1P \rightarrow 1P$ transitions are expected to be considerably further blue-shifted. Thus, both of the energetically lowest-lying electronic transitions in the case of ZnSe quantum dots in thin film form are blue-shifted with respect to the expected transitions in the case of bulk material, but the splitting between them (which is essentially due to the spin-orbit interaction) is essentially unchanged.

It is interesting at this point to address the issue why there is essentially no change in the spin–orbit splitting energy of the valence band components upon particle size reduction (having in mind that the band gap energy itself is significantly affected). The detailed analysis of this issue may be found in the original paper by Chestnoy and coworkers [28]. We here only review the most important points relevant to the problem considered. In the case of three-dimensionally confined ZnSe nanostructures (3D quantum dots) it can be shown by rigorous analysis [28,35] that the bulk ZnSe valence band components Γ_7 and Γ_8 are split into discrete levels which may be characterized with various overall angular momentum, as depicted in Fig. 8. The low-lying $1S$ hole states arising from valence band Γ_7 and Γ_8 components are relatively pure (i.e., do not mix with other, higher angular momentum states) in the case of small nanocrystallites. Both states shift together to higher (in absolute value) energies via the *isotropic* hole mass (not the light or heavy hole mass), as shown by the analyses of Chestnoy and Baldereschi [28,35]. That means that although there is overall band gap blue shift (and thus, a shift in optical transition energies), the splitting between the two transitions (which is essentially of spin–orbit type) remains unchanged.

4.3.2. *Optical properties of thermally annealed thin films. Evolution from size-quantized to bulk optical properties*

Upon thermal annealing of the as-deposited ZnSe thin films, the average crystal size continuously increases, as discussed in Section 4.2. The continual increase of the average crystal size is accompanied with a continual red shift of the absorption onset (Fig. 9). Thus, the films annealed at 250°C are characterized by an absorption onset at ≈475 nm, which is equal to the bulk value. The plot of $(\alpha h\nu)^2$ vs. $h\nu$ in the case of a film

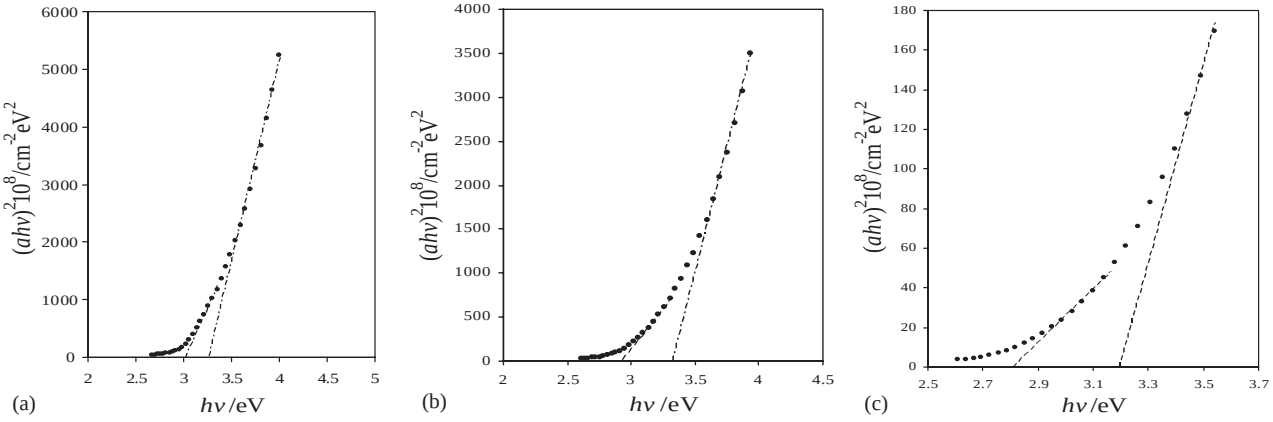

Fig. 9. Evolution of discrete energetic structure of quantum dots to band structure: (a) annealed ZnSe thin film at 100°C, (b) annealed ZnSe thin film at 150°C and (c) annealed ZnSe thin film at 200°C.

annealed at 250°C with thickness of 75 nm is shown in Fig. 10. First of all, it can be seen that the type of transitions is unchanged upon thermal annealing, as well as the order of magnitude of α above the absorption onset. The annealed films are also characterized by direct band-to-band electronic transitions, which are not accompanied by a change in the electron momentum. There are two energetically lowest-lying electronic transitions, one at 2.60 and another one 3.00 eV. The first value corresponds to the band gap value of bulk ZnSe, i.e., using the notation adopted in Refs. [27], to direct transitions from the highest valence band to the lowest conduction band at the Γ point ($\Gamma_{15}^{v} \rightarrow \Gamma_{1}^{c}$ in single-group notation). However, as the spin–orbit interaction splits the Γ_{15}^{v} valence band into Γ_{8}^{v} and Γ_{7}^{v} (with splitting energy Δ_0), the corresponding optical transitions at $k = 0$ (or near $k = 0$) relevant to the present study are: the $\Gamma_{8}^{v} \rightarrow \Gamma_{6}^{c}$, occurring at energy E_g (or also denoted as E_0), and the $\Gamma_{7}^{v} \rightarrow \Gamma_{6}^{c}$ transition, occurring at energy $E_g + \Delta_0 (E_0 + \Delta_0)$. These transitions are denoted with arrows in Fig. 7.

A comparison between the $(\alpha hv)^2$ vs. hv dependencies plotted in Fig. 9 for the cases of ZnSe thin films annealed at various temperatures (i.e., with continually increasing average crystal sizes) shows that the absorption coefficient α at a given photon energy decreases upon average crystal size increase. This is in fact manifested through the decrease of the $(\alpha hv)^2$ values at given photon energies upon average crystal size increase. Although the size dependence of the exciton oscillator strengths in the case nanocrystalline semiconductors is still only partially solved problem, the following arguments may be outlined to explain the experimentally observed situation in our case. The oscillator strength f of the exciton is given by the expression [42]

$$f = \frac{2m}{\hbar^2} \Delta E |\mu|^2 |U(0)|^2, \tag{22}$$

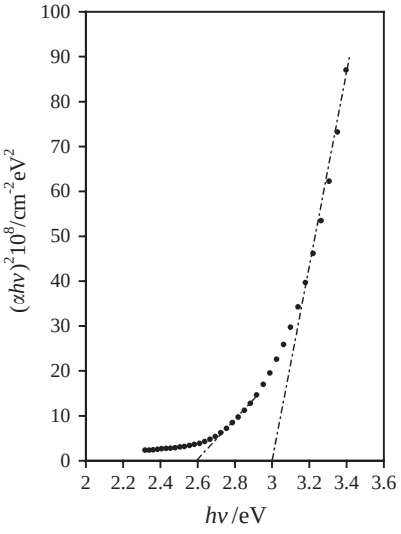

Fig. 10. Dependence of $(\alpha hv)^2$ on hv in the case of annealed ZnSe thin film at 250°C.

where m is the electron mass, ΔE the energy of the transition, μ the transition dipole moment, while $|U(0)|^2$ represents the probability of finding the electron and hole at the same site (a factor of overlap). The absorption coefficient is determined by the ratio of the overall (total) oscillator strength per cluster—f_{cluster} and the cluster volume V (i.e., the ratio f_{cluster}/V). In the case of clusters with radius larger than the Bohr exciton radius ($R \gg r_B$), the overlap factor $|U(0)|^2$ is size-independent, the macroscopic transition dipole moment determining the oscillator strength. On the other hand, in cases when $R < r_B$, $|U(0)|^2$ increases upon cluster volume decrease. Thus, the f_{cluster} value is only weakly dependent on the cluster size in this regime. The absorption coefficient (i.e., the ratio f_{cluster}/V) is thus expected to increase upon decrease of the cluster size.

This is exactly observed in our experiments, although the absorption bands corresponding to excitonic transitions are still wiped away by the continuum absorption, as also explained below.

Regarding the possibility for detection of any indirect electronic transitions in the case of presently studied material, according to the published band structure, the lowest indirect absorption edge of ZnSe may correspond to transitions from the highest valence band at the Γ point to the lowest conduction band at the L or X point (i.e., $\Gamma_8^v \rightarrow L_6^c$ or $\Gamma_8^v \rightarrow X_6^c$). However, according to the previously accumulated experimental and theoretical evidence, the lowest direct band gap E_0 in the case of ZnSe should always be (i.e., regardless on the external conditions) lower than the indirect band gaps (e.g., for 1.0 eV at zero pressure). As the strengths of indirect transitions are always weaker than the direct ones, they are expected to be overwhelmed by the direct gap contributions. The absence of any indirect electronic transitions (accompanied by a change in electronic momentum) in the presently studied system is thus in fact expected.

It seems important at this point to discuss another interesting aspect related to the optical properties of nanocrystalline ZnSe deposited in thin film form. It has been recently shown in several studies that certain interdot electronic coupling may occur in the case of close-packed quantum dot solids [43–48]. According to the recently accumulated data [43–48], such coupling would be expected to occur only between very closely packed and very small quantum dots, mainly by tunneling mechanism, in which the charge carrier leakage outside the nanoparticle is significant. This interdot coupling is manifested in the optical properties of the solid materials through the exciton peak broadening (in comparison to the case of diluted ensembles of quantum dots). In the case of our as-deposited ZnSe quantum dots in thin film form, the non-observance of clearly defined excitonic absorption peaks, besides to other relevant reasons, may be attributed partly due to exactly such additional broadening occurring as a result of interdot electronic couplings. In other words, the observance of a structureless absorption spectrum in the case of our chemically deposited ZnSe quantum dot thin films may be attributed to the formation of collective electronic states in an ensemble of quantum dots. These states, which are delocalized within a finite number of nanocrystals are formed due to the interdot electronic coupling. In the case of annealed materials, however, similarly as in the case of CdSe quantum dots, the possibility of interdot electronic coupling would be expected to be significantly reduced due to the crystal size increase as a result of sintering. All these conclusions are in line with the recent observations of the effects of interdot electronic coupling on the optical absorption properties of various close-packed ultrasmall quantum dot solids [43–48].

4.4. Analysis of the three-dimensional quantum confinement effects in ZnSe quantum dots in thin film form

4.4.1. The Brus (effective mass approximation) model

The three-dimensional quantum confinement effects in semiconducting nanocrystals (i.e., the quantum size effects) have been recognized and correctly understood and interpreted almost two decades ago [49]. However, effective usage of these effects in band gap design and engineering dates from much later. Also, development of an exact theoretical model which would give quantitative agreement of the predicted dependence of E_g on the crystal size remains a task which is still only partially solved. Therefore, comparing new experimental data for a variety of semiconducting nanocrystals with the predictions of various theoretical models is still of significant importance for semiconductors science and technology and for the solid state physics and chemistry in general.

One of the most widely used theoretical models which allows a relatively simple analytical formula for the dependence of E_g on R (crystal size) to be derived is the much quoted Brus model [50,51]. According to this model, the band gap of a semiconducting (nano)crystal considered as a sphere with radius R is given by

$$E_g(R) = E_{g,bulk} + \frac{h^2}{8m_0R^2}\left(\frac{1}{m_e^*}+\frac{1}{m_h^*}\right) - \frac{1.8e^2}{4\pi\varepsilon_0\varepsilon_r R} - 0.248\frac{4\pi^2e^4m_0}{2(4\pi\varepsilon_0\varepsilon_r)^2h^2\left(\frac{1}{m_e^*}+\frac{1}{m_h^*}\right)}, \quad (23)$$

where $E_{g,bulk}$ is the bulk crystal band gap value, i.e., the limit towards which the $E_g(R)$ converges upon increase of the crystal radius R, h is the Planck's constant, m_0 is the electron mass, while m_e^* and m_h^* are the electron and hole relative effective masses, respectively (i.e., the effective masses expressed in units of m_0), e is the electron charge, ε_0 the permitivity of vacuum and ε_r the relative dielectric constant of the semiconductor (usually taken as the bulk $\varepsilon_{r,\infty}$ value or the static $\varepsilon_{r,s}$ value). The band gap shift with respect to the bulk value is, thus

$$\Delta E_g(R) = \frac{h^2}{8m_0R^2}\left(\frac{1}{m_e^*}+\frac{1}{m_h^*}\right) - \frac{1.8e^2}{4\pi\varepsilon_0\varepsilon_r R} - 0.248\frac{4\pi^2e^4m_0}{2(4\pi\varepsilon_0\varepsilon_r)^2h^2\left(\frac{1}{m_e^*}+\frac{1}{m_h^*}\right)}. \quad (24)$$

The first term on the right-hand side of Eq. (24) is the quantum localization term (i.e., the kinetic energy term), which shifts the $E_g(R)$ to higher energies proportionally to R^{-2}. The second term in (24) is due to the screened Coulomb interaction between the electron and the hole, and it shifts the $E_g(R)$ to lower energies as R^{-1}. The third, size-independent term in (24) is due to spatial

correlation effects, and is usually small in both the absolute value and also in the sense of its contribution to overall $\Delta E(R)$. However, for semiconductors with small ε_r values it may become significant in both senses, especially its contribution to the overall $\Delta E(R)$ in cases when conditions are fulfilled so that the opposite trends induced by quantum localization and Coulomb terms tend to cancel.

In the case of presently studied system, we have studied the dependence of band gap value on crystal size (R) upon annealing of ZnSe nanocrystals deposited in thin film form at various temperatures. The band gap value of as-deposited ZnSe (from bath containing zinc sulfate as a source of Zn^{2+} ions), with average crystal size of 1.4 nm is 3.10 eV, which is blue-shifted by 0.52 eV as compared to the band gap value of bulk ZnSe (2.58 eV). The theoretically predicted band gap blue-shift according to the Brus model for this crystal size is 1.22 eV, which is obviously much too high in comparison to the experimental data. For crystal size of 1.4 nm, the quantum localization contribution to overall $\Delta E(R)$ is $\Delta E_{q.l.} = 1.45$ eV, the screened Coulomb contribution is $\Delta E_{Coulomb} = -0.23$ eV, while the size-independent spatial correlation term is indeed negligible $-\Delta E_{s.c.} = -0.0068$ eV. The predominance of the kinetic quantum localization term in the overall $\Delta E(R)$ value, accompanied with the negligible $\Delta E_{s.c.}$ contribution may be attributed to the relatively high ε_r value for Bulk ZnSe—8.1. The discrepancy between the predictions of the Brus model and the experimental data remain even for larger R values. Thus, for thin film samples annealed at 200°C characterized with average crystal radius of 1.8 nm, the experimentally obtained $\Delta E(R)$ is 0.32 eV, while the theoretically predicted value is 0.70 eV. Further annealing of the thin film samples at 250°C leads to irreversible disappearance of the confinement effects—i.e., in this case the average crystal size increases to 2.0 nm, which further downshifts the experimental band gap energy to 2.60 eV, which is higher by only 0.02 eV with respect to the bulk value, while the Brus model predicts a band gap energy upshift of 0.55 eV for such R value. Thus the results obtained in the present study for ZnSe nanocrystals are significantly different from those recently reported by our group for CdSe quantum dots in thin film form [11,12]. In the case of CdSe thin films, the agreement between the predictions of the Brus model and our experimental data, although being rather weak for the smallest CdSe nanocrystals deposited in thin film form, became much better upon crystal size increase due to thermal annealing. Thus, in the case of CdSe, we attributed the disagreement between the Brus model and experiment in the case of rather low R values to the inadequacy of the effective mass approximation (i.e., the parabolic band approximation, as the effective mass approximation is equivalent to considering the energy surfaces of the parabolic form $\hbar^2k^2/(2m^*)$) on which this theoretical model is implicitly based. As the crystal size increases, the approximation becomes more and more valid, and so the agreement with the experimental data.

According to the effective mass approximation, the quantum confinement effects should be clearly observable if the cluster radius becomes less than Bohr excitonic radius for the corresponding material, given by the following relation:

$$r_B = \frac{4\pi\varepsilon_0\varepsilon_r\hbar^2}{e^2 m_0}\left(\frac{1}{m_e^*} + \frac{1}{m_h^*}\right). \quad (25)$$

In the last equation, r_B is the bulk Bohr excitonic radius, while all other symbols have the same meaning as in the previous equations. Using the corresponding parameters for ZnSe, the estimated value for r_B in the case of this material is 3.2 nm, which is quite in line with our experimental data—the three-dimensional quantum confinement effects should be quite pronounced in the case of nanocrystals with radii smaller than r_B. The previously estimated literature values for r_B of 9 nm [52] thus seems to be too high.

4.4.2. The hyperbolic band model

Generally speaking, there are two main reasons that could be responsible for inadequacy of the Brus model for quantitative description of the quantum confinement effects in nanocrystals. The first one is the breakdown of the effective mass approximation upon crystal size decrease, and the second one is the size-dependence of the Coulomb interaction. Regarding the first possibility, in order to test whether the parabolic band approximation is the main reason behind the inadequacy of the Brus model in describing the electronic properties of ZnSe nanocrystals, we tested the applicability of the hyperbolic band model, originally developed and applied for PbS semiconducting nanocrystals [53] to the presently studied system. This model is based on two main approximations. The first one presumes that the basic lattice excitation of a semiconductor of the type MA involves a charge transfer from the anion to the metal cation, at a cost in energy equal to the bulk band gap E_g. The second approximation inherent to the hyperbolic band model is that it accounts only for *two* relevant bands for calculation of the band gap energy—those which at the relevant point of the Brillouin zone correspond to the highest occupied valence band and the lowest unoccupied conduction band. Neglecting the Coulomb corrections to the overall band gap shift (presumed to be small within this model), the following analytical formula may be derived for the size-dependent band gap energy $E(R)$:

$$E(R) = \sqrt{E_g^2 + \frac{2\hbar^2 E_g \pi^2}{m_0 R^2}\frac{1}{2}\left(\frac{1}{m_e^*} + \frac{1}{m_h^*}\right)}, \quad (26)$$

where $\hbar = h/(2\pi)$, while all the other terms have identical meaning as in Eqs. (23)–(25). The main improvement of the hyperbolic band model over the model of Brus is that the former accounts for the electron and hole band non-parabolicity—thus, the hole and electron bands, within this model, are hyperbolic, but approaching parabolic behavior at Γ point. Within this model, the predicted $\Delta E(R)$ values for $R = 1.4$, 1.8 and 2.0 nm are 1.18, 0.76 and 0.63 eV, so that (except for the first value) the agreement with the experimental data is quite similar as in the case of Brus model. A straightforward conclusion which may be derived from the presented data is that the electron and hole band non-parabolicity cannot be the main reason for the disagreement between theory and experiment. If one simply adds the Coulomb term from the Brus model to the hyperbolic band model $\Delta E(R)$ values (as this model does not include the screened Coulomb interaction between electrons and holes at all), the following $\Delta E(R)_{\mathrm{HBM+Coulomb}}$ values are obtained for $R = 1.4$, 1.8 and 2.0 correspondingly: 0.95, 0.59 and 0.47 eV. The agreement with the experimental data is thus much better, but still not satisfactory. This could not be, however, expected, since the $\Delta E(R)_{\mathrm{HBM+Coulomb}}$ values have been obtained by a quite, in a sense, artificial procedure.

The second, and (as we'll see in what follows) the key reason behind the disagreement between theory and experiment in the cases of both the effective mass model (or Brus model) and the hyperbolic band model lies in the inappropriate treatment of the screened Coulomb interaction in both cases. While the hyperbolic band model does not account for the Coulomb interaction at all, the Brus model accounts for it via the second term in Eqs. (24) and (25). However, as mentioned before, the relative dielectric constant of the semiconductor ε_r is usually taken as the *bulk* $\varepsilon_{r,\infty}$ value (or the static *bulk* ε_r value). On the other hand, as elaborated in the exciton literature, it is possible that the effective dielectric constant of a semiconducting material becomes reduced in the case of sufficiently small particles. This effect is believed to be due to the fact that dielectric screening decreases with exciton radius as a result of the inability of the lattice polarization to follow the more rapid electron and hole motion associated with a smaller radius. If the previous statement is taken to be true, then by simply "correcting" the used ε_r value in effective mass approximation, one should expect that Brus model should account properly for $\Delta E(R)$ regardless on the value of R itself. We have found that setting the ε_r value in Eq. (24) to 2.0, leads to an excellent agreement between the predictions of the Brus model and the experimental data. For R values of 1.4, 1.8 and 2.0, the corresponding $\Delta E(R)$ values according to this corrected model are 0.52, 0.16 and 0.06 eV, which is in excellent agreement with the experimental data (the corresponding values being 0.52, 0.22 and 0.02 eV). We will elaborate in much more details the results from all of these calculations, according to the various theoretical models considered, in a forthcoming publication [54].

4.5. Electrical properties of zinc selenide thin films

For investigation of electrical properties of zinc selenide thin films, achievement of ohmic contact between investigated thin film sample and used silver paste is necessary. The ohmic type of silver–zinc selenide contact was proved on the basis of linear dependence of electrical current on the applied voltage.

On the basis of negative sign of the thermoelectric force of zinc selenide–metal thermocouple, we have concluded that zinc selenide is *n*-type semiconductor and the dominant charge carriers are free electrons. This conclusion is in agreement with the theoretical predictions, since the effective electron mass is smaller than effective hole mass ($m_e^* < m_h^*$) [15] for this semiconductor.

As-deposited ZnSe thin films are highly resistive. Their room temperature dark electrical resistance is of the order of GΩs, depending on film thickness and preparative conditions. As was previously discussed, the as-deposited thin films are strongly quantized. The high dark electrical resistance goes in contribution of the above discussion. The free electrons and holes are physically confined within the zinc selenide quantum dots. The electrical isolation between zinc selenide quantum dots deposited as (macroscopically "continual") thin films implies a large potential barrier between them. Annealing process of prepared thin films leads to exponential decrease of their dark electrical resistance which is in correlation with the expectations based on semiconductor physics and expected increase of crystal size (as a result of coalescence processes during thermal treatment) as well. Temperature dependence of dark electrical resistance of the investigated thin film samples was measured in inert (argon) atmosphere up to 380°C. The purpose of these measurements was to get additional information about the band structure of investigated semiconductor in thin film form, especially regarding the so-called band gap states. According to the solid-state physics of semiconductors, the temperature dependence of electrical conductivity (σ) of an extrinsic semiconductor is determined by the following equation:

$$\sigma = \sigma_0 T^{(3/2)} e^{-(E_g/2kT)} + \sigma_0' e^{-(\Delta E/kT)}, \quad (27)$$

where σ_0 and σ_0' are constants, k is Boltzmann constant and E_g and ΔE are band gap energy and ionization energy of impurity level, correspondingly. The first term of this equation corresponds to interband electronic transitions (i.e., mechanism of intrinsic conductivity) while the second term corresponds to electronic transitions from donor levels to conduction band (in the case of *n*-type semiconductors) or to electronic transitions from

valence band to acceptor levels (in the case of *p*-type semiconductors). Having in mind the above equation, on the basis of experimentally obtained data, the $\ln(R/\mathrm{k}\Omega)$ vs. $10^3 T^{-1}/\mathrm{K}^{-1}$ dependence was plotted in Fig. 11. As can be seen from this figure one linear trend was observed. The decrease of thin film electrical resistance in the investigated temperature region is due to mechanism of extrinsic (or impurity) conductivity. The experimental data were fitted by the following function:

$$\ln R = \frac{\Delta E}{kT} + \ln R_0. \tag{28}$$

The calculated ionization energy of impurity level at 0 K is 0.82 eV. According to this finding, it can be concluded that there is a deep impurity (donor) level in the forbidden band gap of zinc selenide in thin film form as has been proposed by Bube [55]. In Fig. 12 the dependence of $\ln(R/\mathrm{k}\Omega)$ vs. $10^3 T^{-1}/\mathrm{K}^{-1}$ during a single heating–cooling process is presented. The temperature dependence of dark electrical resistance was measured for zinc selenide samples prepared under different experimental conditions. Significant differences in ionization energy of impurity level due to using different zinc salt as a zinc ion precursor were not detected.

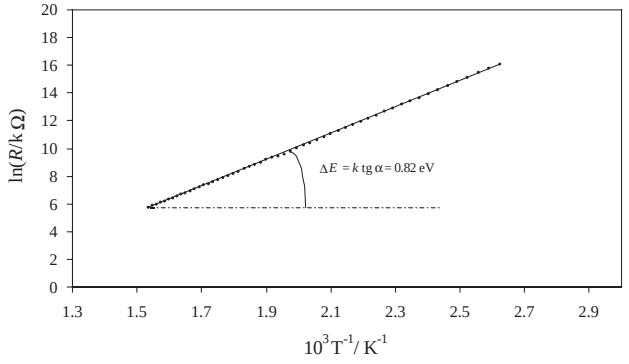

Fig. 11. Dependence of $\ln R$ on $1/T$ in the region of extrinsic conduction for ZnSe thin film.

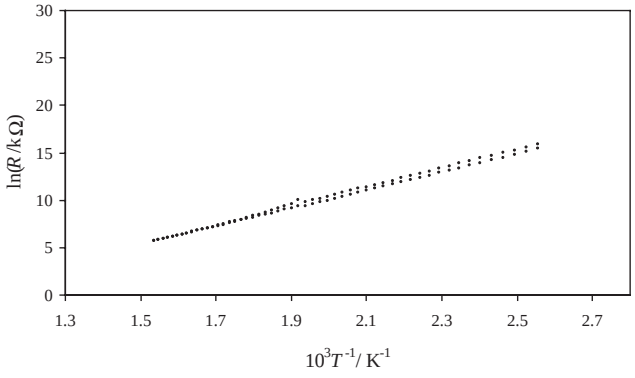

Fig. 12. Dependence of $\ln R$ on $1/T$ in the region of extrinsic conduction for ZnSe thin film during a single heating–cooling process.

Since ZnSe is a large band gap semiconducting material, in order to determine the E_g value from thermal measurements, rather high temperature values should be achieved ($>400^\circ$C). At such high temperatures, however, the glass substrates undergo a large viscosity change, so the precise measurements of the resistivity of the semiconducting thin film deposited onto the substrate surface become essentially impossible. However, the E_g value has been determined from optical measurements for both the as-deposited and the thermally annealed samples (at room temperature).

5. Conclusions

We have presented a novel, convenient chemical method for deposition of zinc selenide quantum dots in thin film form, with potential applications in microelectronics and solar cell engineering. The obtained films are cubic and behave as intrinsic semiconductors. Band gap energy of as-deposited three-dimensionally confined ZnSe quantum dots is strongly blue-shifted with respect to the bulk value, but the spin–orbit induced splitting of the valence band remains essentially unchanged in the course of electron and hole confinement. The two electronic transitions observed at 3.10 and 3.50 eV in the case of strongly quantized ZnSe films are attributed to the existence of two discrete states originating from the valence band spin–orbit components. Upon annealing at 250°C, the band gap energy of the deposited films converges to the value for bulk ZnSe, with the spin–orbit splitting of the valence band of 0.40 eV. The band gap decrease is accompanied with an increase of the average crystal size of the films, lattice strain relaxation, and lattice constant enlargement. Although the effective mass approximation model does not lead to a quantitative agreement with the experimental data for the band gap blue shift when bulk ZnSe relative dielectric constant is used, somewhat smaller values for this constant allow for a quantitative agreement with the experiment. This implies that the relative dielectric constant of this material in nanocrystalline form could be as much as four times smaller than the bulk value, in line with some previous estimations. The inadequacy of the hyperbolic band model to predict quantitatively the band gap dependence on the crystal size in the case of the studied material further supports the previous statement. On the basis of the measured temperature dependence of the dark electrical resistivity of annealed thin films, ionization energy of a deep donor impurity level of 0.82 eV at 0 K is calculated.

References

[1] T. Trinade, P. O'Brien, N.L. Pickett, Chem. Mater. 13 (2001) 3843.

[2] R.F. Khairrutdinov, Russ. Chem. Rev. 67 (1998) 109.
[3] B. O'Regan, M. Grätzel, Nature 353 (1991) 737.
[4] V.L. Colvin, M.C. Schlamp, A.P. Alivisatos, Nature 370 (1994) 354.
[5] A. Hagfeldt, N. Vlachopoulos, M. Grä[al]tzel, J. Electrochem. Soc. 141 (1994) L82.
[6] T.S. Kang, D. Kim, K.J. Kim, J. Electrochem. Soc. 145 (1998) 1982.
[7] B. Pejova, M. Najdoski, I. Grozdanov, S.K. Dey, J. Mater. Chem. 9 (1999) 2889.
[8] B. Pejova, M. Najdoski, I. Grozdanov, S.K. Dey, Mater. Lett. 45 (2000) 2694.
[9] B. Pejova, I. Grozdanov, J. Solid State Chem. 158 (2001) 49.
[10] B. Pejova, I. Grozdanov, Thin Solid Films 408 (2002) 6.
[11] B. Pejova, A. Tanuševski, I. Grozdanov, J. Solid State Chem. 172 (2003) 381.
[12] B. Pejova, A. Tanuševski, I. Grozdanov, J. Solid State Chem. 174 (2003) 276.
[13] B. Pejova, I. Grozdanov, Mater. Lett. 58 (2004) 666.
[14] B. Pejova, I. Grozdanov, A. Tanuševski, Mater. Chem. Phys., in press.
[15] A.B. Novoselova (Ed.), Physical and Chemical Properties of Semiconductors, Handbook Moscow, 1978.
[16] S.A. Empedocles, D.J. Norris, M.G. Bawendi, Phys. Rev. Lett. 77 (1996) 3873.
[17] C.C. Kim, S. Sivananthan, Phys. Rev. B 53 (1996) 1475.
[18] Y. Ohtake, T. Okamoto, A. Yamada, M. Kongai, K. Saito, Sol. Energy Mater. Sol. Cells 49 (1997) 2699.
[19] A.K. Turner, J.M. Woodcock, M.E. Özsan, et al., Sol. Energy Mater. Sol. Cells 35 (1994) 263.
[20] P. Pramanik, S. Biswas, J. Electrochem. Soc.: Electrochem. Sci. Tech. (1986) 350.
[21] G.N. Chaudhari, S. Manorama, V.J. Rao, J. Phys. D 25 (1992) 862.
[22] C.A. Estrada, P.K. Nair, M.T.S. Nair, R.A. Zingaro, E.A. Meyers, J. Electrochem. Soc. 141 (1994) 802.
[23] J.M. Doña, J. Herreo, J. Electrochem. Soc. 142 (1995) 764.
[24] C.D. Lokhande, P.S. Patil, A. Ennaoui, H. Tributsch, Appl. Surf. Sci. 123/124 (1998) 294.
[25] Handbook of Chemistry and Physics, 64th edition, CRC Press, Boca Raton, FL, 1983–1984.
[26] Microsoft® EXCEL 97 SR-1.
[27] S. Adachi, Mater. Chem. Phys. 83 (2004) 245.
[28] N. Chestnoy, R. Hull, L.E. Brus, J. Chem. Phys. 85 (1986) 2237.
[29] B. Pejova, I. Grozdanov, Appl. Surf. Sci. 177 (2001) 152.
[30] G.M. Fofanov, G.A. Kitaev, Russ. J. Inorg. Chem. 14 (1969) 322.
[31] D.A. Davies, A. Vecht, J. Silver, P.J. Marsh, J.A. Rose, J. Electrochem. Soc. 147 (2000) 765.
[32] M.T. Weller, Inorganic Materials Chemistry, Oxford University Press, Oxford, 1997.
[33] JCPDS—International Center for Diffraction Data 37-1463.
[34] S. Gorer, G. Hodes, J. Phys. Chem. 98 (1994) 5338.
[35] J.A. Venables, Introduction to Surface and Thin Film Processes, Cambridge University Press, Cambridge, 2000.
[36] M. Ohring, The Materials Science of Thin Films, Academic Press, San Diego, 1992.
[37] A.R. Stokes, in: H. S. Peiser, et al. (Eds.), X-Ray Diffraction by Polycrystalline Materials, Chapman & Hall, London, 1960.
[38] W.D. Callister, Materials Science and Engineering—an Introduction, Wiley, New York, 1997.
[39] S. Velumani, Sa.K. Narayandass, D. Mangalaraj, Semicond. Sci. Technol. 13 (1998) 1016.
[40] B. Abay, H.S. Güder, H. Efeoğlu, Y.K. Yoğurtçu, Semicond. Sci. Technol. 15 (2000) 535.
[41] M.P. Marder, Condensed Matter Physics, Wiley, New York, USA, 2000.
[42] Y. Wang, N. Herron, J. Phys. Chem. 95 (1991) 525.
[43] D.I. Kim, M.A. Islam, L. Avilla, I.P. Herman, J. Phys. Chem. B 107 (2003) 6318.
[44] M.V. Artemyev, A.I. Bibik, L.I. Gurinovich, S.V. Gaponenko, H. Jaschinski, U. Woggon, Phys. Stat. Sol. (B) 224 (2001) 393.
[45] O.I. Micic, S.P. Ahrenkiel, A.J. Nozik, Appl. Phys. Lett. 78 (2001) 4022.
[46] M.V. Artemyev, U. Woggon, H. Jaschinski, L.I. Gurinovich, S.V. Gaponenko, J. Phys. Chem. B 104 (2000) 11617.
[47] B.S. Kim, L. Avila, L.E. Brus, I.P. Herman, Appl. Phys. Lett. 76 (2000) 3715.
[48] M.V. Artemyev, A.I. Bibik, L.I. Gurinovich, S.V. Gaponenko, U. Woggon, Phys. Rev. B 60 (1999) 1504.
[49] L.E. Brus, J. Chem. Phys. 79 (1983) 5566.
[50] L.E. Brus, J. Chem. Phys. 80 (1984) 4403.
[51] L.E. Brus, J. Phys. Chem. 90 (1986) 2555.
[52] N. Kumbhojkar, S. Mahamuni, V. Leppert, S.H. Risbud, Nanostruct. Mater. 10 (1998) 117.
[53] Y. Wang, A. Suna, W. Mahler, R. Kasowski, J. Chem. Phys. 87 (1987) 7315.
[54] B. Pejova, I. Grozdanov, Mater. Chem. Phys., in press.
[55] R.H. Bube, E.L. Lind, Phys. Rev. 110 (1958) 1040.